Available online at www.sciencedirect.com

SciVerse ScienceDirect

Ceramics International 39 (2013) 1371–1377

CERAMICS INTERNATIONAL

www.elsevier.com/locate/ceramint

The effect of group-I elements on the structural and optical properties of ZnO nanoparticles

Ramin Yousefi[a,*], A.Khorsand Zak[b], Farid Jamali-Sheini[c]

[a]Department of Physics, Masjed-Soleiman Branch, Islamic Azad University (I.A.U.), Masjed-Soleiman, Iran
[b]Materials and Electroceramics Laboratory, Department of Physics, Faculty of Science, Ferdowsi University of Mashhad, Iran
[c]Department of Physics, Ahwaz Branch, Islamic Azad University, Ahwaz, Iran

Received 8 June 2012; received in revised form 23 July 2012; accepted 23 July 2012
Available online 31 July 2012

Abstract

Undoped and group-I elements doped ZnO nanoparticles (NPs) ($Zn_{1-y}X_{2y}O$, X=Li, Na, K, and $y=0.05$) were synthesized by a sol–gel method. Structural and morphological studies of the resulting products were carried out by X-ray diffraction analysis (XRD) and transmission electron microscopy (TEM). The XRD results revealed that the sample products were crystalline with a hexagonal wurtzite phase. The TEM images showed ZnO NPs with nearly spherical shapes with particle size distributed over the nanometer range. In addition, the XRD and TEM results showed a decrease in crystallite and particle sizes of NPs from Li-doped to K-doped ZnO NPs. Crystalline development in the ZnO NPs was investigated by X-ray peak broadening. The size-strain plot (SSP) method was used to study the individual contributions of crystallite sizes and lattice strain on the peak broadening of the undoped and doped ZnO NPs. The effect of doping on the optical band-gap and crystalline quality was also investigated by using photoluminescence (PL) and Raman spectrometers. The Raman spectra of the all ZnO NPs showed a strong E_2(high) peak. The PL spectra exhibited a strong peak in the ultraviolet (UV) region of the electromagnetic spectrum for the all ZnO NPs. The UV peak of the doped ZnO NPs was red-shifted with respect to that of the undoped ZnO NPs.

Keywords: C. Optical properties; ZnO nanoparticles; Structural properties; Group-I elements-doped ZnO

1. Introduction

Zinc oxide can be used in many applications, including transparent conductive coatings [1], electrodes for dye-sensitized solar cells [2], gas sensors [3], and field emission materials [4]. Apart from the technological significance of ZnO nanostructures, their quasi-one-dimensional structure with diameters in the range of tens of nanometers to hundreds of nanometers makes them interesting from a scientific point of view. In this size range, they are expected to possess interesting physical properties and pronounced coupling quite different from their bulk counterpart [5]. In order to obtain better crystallization quality, optical, electrical, and ferromagnetic properties, researchers carried out doping in ZnO. We also have reported several studies about different kinds of doping materials as a donor in ZnO nanomaterials to obtain high quality *n*-type ZnO nanomaterials, and studied effect of these materials on optical and electrical properties of ZnO nanomaterials [6–9]. However, the key challenge that needs to be overcome for the realization of most ZnO based applications is the fabrication of *p*-type material. *P*-type ZnO may be achieved by the substitution of group-I elements on Zn-site [10–12] and group-V elements on O-site [13–15], respectively. Although significant progress has been made recently full control over the materials conductivity type is still to be obtained and hence a comprehensive investigation of the fundamental properties of acceptors in ZnO is needed. Group-I elements are better dopants materials than group-V elements in terms of the shallowness of the accepter level [16]. Therefore, the study of different effects

*Corresponding author. Tel.: +98 9166224993; fax: +98 6813330093.
E-mail address: yousefi.ramin@gmail.com (R. Yousefi).

0272-8842/$ - see front matter © 2012 Elsevier Ltd and Techna Group S.r.l. All rights reserved.
http://dx.doi.org/10.1016/j.ceramint.2012.07.076

of group-I elements as dopants on structural and optical properties of ZnO nanostructures can lead to obtain *p*-type ZnO nanostructures.

Several groups and researchers have tried to obtain *p*-type ZnO nanostructures by employing group-I elements as acceptors. Jayanthi and co-workers compared the effects of Li and Na on the morphology of ZnO nanocrystals. They found that lattice parameters and bond length of Li- and Na-doped ZnO nanocrystals were altered due to different ionic radii of Li^+ and Na^+ [10]. Huang et al. performed a systematic study of diffusion Li, Na, and K in ZnO based on ab initio total energy calculations. They found that interstitial K has a relatively smaller energy barrier than Li and Na [12]. In addition, Lee and Chang investigated possible *p*-type doping with group-I elements in ZnO. They found that Li and Na are better acceptors with shallower acceptor levels than N, while they are mostly self-compensated by Li and Na interstitials, respectively. They also found that a co-doping with H impurities and a subsequent annealing process greatly enhance the electrical activity of group-I dopants [17]. Xiao et al. doped ZnO with Li using pulsed laser deposition (PLD). They concluded that Li-doped ZnO thin film not only provided good *p*-type behavior but also showed high transmittance in the visible region [18]. In addition, a Li–N dual-acceptor doping method has been developed by Lu and co-workers to prepare *p*-type ZnO thin films using PLD [19]. They observed much lower resistivity for Li–N co-doped ZnO thin film than that of Li or N monodoped ZnO films. We believe that although the researches on the effect of group-I elements on optical and electrical of ZnO has been performed, but the effects of group-I elements on structural properties of ZnO have not been reported to date. Therefore, the study of different effects of group-I elements on structural and optical properties of ZnO nanostructures can lead to better understanding of the behavior of these materials as acceptors in ZnO structure. Such knowledge can enhance development of optoelectronic devices in the future.

For these reasons, the undoped, Li-, Na-, and K-doped ZnO-NPs were prepared by a sol–gel method using gelatin as stabilizer in the present work. We report a comparative study of the effects of group-I elements on the structural and optical properties of the ZnO nanoparticles.

2. Experimental

To begin the synthesis of Na- and K-doped ZnO-NPs, analytical grade zinc nitrate hexahydrate ($Zn(NO_3)_2 \cdot 6H_2O$), lithium nitrate ($LiNO_3$, $>99\%$), sodium nitrate ($NaNO_3$, $>99\%$), potassium nitrate (KNO_3, $>99\%$), gelatin (type B from bovine skin) and distilled water were used as starting materials. All of the materials used were purchased from Sigma-Aldrich. The precursors were measured as $Zn_{1-y}X_{2y}O$, (X=Li, Na, and K, and $y=0.05$) to obtain 5 g of final product. First, a gelatin solution was prepared by adding gelatin to distilled water at 60 °C. The metal nitrates were separately dissolved in a minimal amount of distilled water at room temperature then added to the gelatin solution. After that, the compound solutions were stirred and heated at 80 °C until honey-like gels were obtained. The gels were calcined at 650 °C for 2 h at a heating rate of 2 °C/ min. The resulting powders were characterized by several tools to check their qualities.

XRD (Philips, X'Pert, CuKa), was used to evaluate phase characteristics of the samples and the TEM observations were carried out on a Hitachi H-7100 electron microscope to examine the shape and particle size of the nanoparticles. Elemental analyses of the products were undertaken using field emission Auger electron spectroscopy (FEAES, JAMP-9500F). Optical properties of the ZnO-NPs were finally characterized by a room temperature photoluminescence spectrometer (PL, Jobin Yvon Horiba HR 800UV, He–Cd laser, 325 nm), and a Raman spectrometer (Jobin Yvon Horiba HR 800UV, Ar ion laser, 514.5 nm).

3. Results and discussions

3.1. X-ray diffraction analysis

Fig. 1. shows the XRD patterns of the prepared samples in the range $2\theta=20^\circ-100^\circ$. All detectable peaks are from

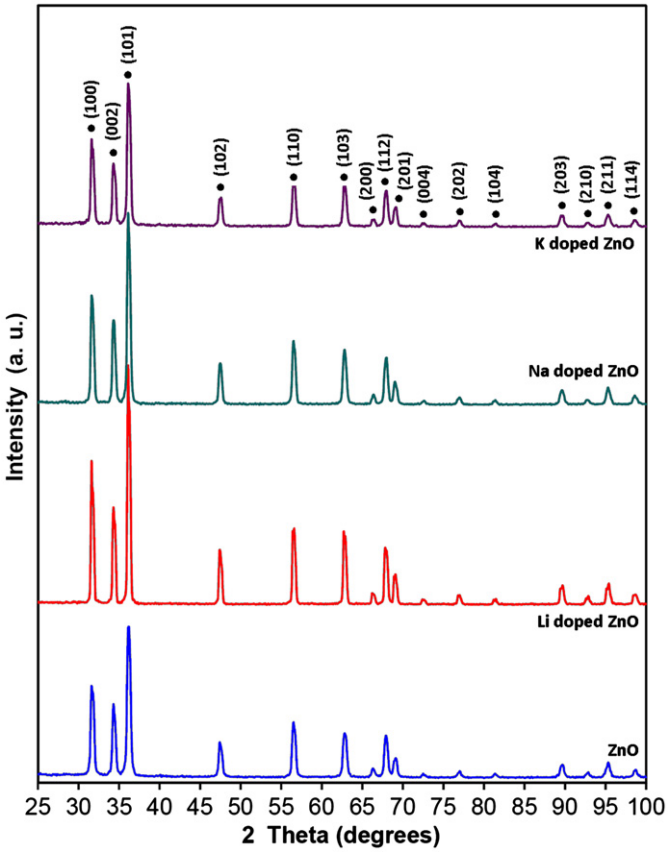

Fig. 1. The XRD patterns of doped and undoped ZnO NPs calcined at 650 °C.

the ZnO wurtzite structure (PDF Card no.: 00-005-0664). There are no other peaks related to Li_2O, Na_2O, K_2O, or other mixed compounds. The intensity of the XRD patterns peaks is greater in the doped samples than in the undoped ZnO-NPs. The maximum peak intensity occurred in Li-doped ZnO NPs, and was significantly less in the Na- and K-doped ZnO NPs. The wurtzite lattice parameters were calculated from the Lattice Geometry equation [20]. The (100) and (002) planes were used to calculate the lattice parameters of the undoped and doped ZnO NPs. Results are summarized in Table 1.

where A is a constant, equal to 4/3 for the spherical shape samples used in this experiment. In Fig. 2 the term $(d_{hkl}\beta_{hkl}\cos\theta)^2$ is plotted with respect to $(d^2_{hkl}\beta_{hkl}\cos\theta)$ for all the diffraction peaks of undoped and doped ZnO NPs from $2\theta = 20^\circ$ to 100°. The crystallite size and strain can be obtained from the slope and root of the y-intercept of the linearly fitted data, respectively. According to Hook's law, for small dislocations in a lattice a linear relation between the stress and strain is given as $\sigma = Y\varepsilon$, where Y is Young's modulus and σ is lattice stress. For a hexagonal structure, Young's modulus can be obtained from the following relation [23].

$$Y_{hkl} = \frac{[h^2 + ((h+2k)^2/3) + (al/c)^2]^2}{s_{11}(h^2 + ((h+2k)^2/3))^2 + s_{33}(al/c)^4 + (2s_{13} + s_{44})(h^2 + ((h+2k)^2/3))(al/c)^2} \quad (3)$$

Usually, the crystallite size is calculated by the Scherrer equation: $D = (k\lambda/\beta_{hkl}\cos\theta)$, where D is the crystallite size in nanometers, λ is the wavelength of the radiation (1.54056 Å for CuK_α radiation), k is a constant equal to 0.94, β_{hkl} is the peak width at half-maximum intensity, and θ is the peak position. However, some parameters affect the peak width. The most important of these parameters is lattice strain, which affects the peak width. There are a number of methods used to calculate the effect of lattice strain on broadening of the lattice diffraction peaks such as the Williamson–Hall and size strain plot (SSP) methods [21]. The SSP method is more accurate, especially at higher diffraction angles. Therefore, the crystallite size and lattice strain of the samples were calculated using the size strain plot (SSP) method. In this method, the peak broadening due to the lattice strain is estimated from $\varepsilon = \beta_s/\tan\theta$ [22]. Therefore, the total broadening is obtained from

$$\beta_{hkl} = \beta_s + \beta_D \quad (1)$$

where β_D is the peak broadening that is corresponding to crystallite size. According to the SSP method, the relation between lattice strain and crystallite size is given by:

$$(d_{hkl}\beta_{hkl}\cos\theta)^2 = \frac{A}{D}(d^2_{hkl}\beta_{hkl}\cos\theta) + \left(\frac{\varepsilon}{2}\right)^2 \quad (2)$$

In the earlier work, the values of s_{11}, s_{13}, s_{33}, and s_{44}, (the lattice compliances of ZnO), were found to be 7.858×10^{-12}, -2.206×10^{-12}, 6.940×10^{-12}, and $23.57 \times 10^{-12}\ m^2\ N^{-1}$, respectively [24]. For an elastic system, which approximately fallows Hooke's law, the energy per unit of a lattice can be calculated from $u = (\varepsilon^2 Y_{hkl})/2$. The crystallite size ($D$), strain ($\varepsilon$), stress ($\sigma$), Young's modulus ($Y$), and energy density ($u$) of

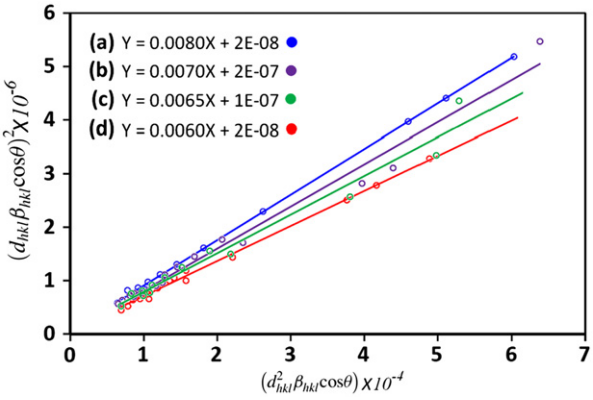

Fig. 2. The SSP plot of (a) ZnO, (b) $Zn_{0.95}K_{0.1}O$, (c) $Zn_{0.95}Na_{0.1}O$, and (d) $Zn_{0.95}Li_{0.1}O$. The particle size is achieved from the slope of the linearly fitted data while the root of the y-intercept gives the strain.

Table 1
The structure parameters of undoped and doped ZnO NPs calcined at 650 °C.

Compound	$2\theta \pm 0.01$	hkl	d_{hkl} (nm) $\pm$ 0.0005	*Structure*	*Lattice parameter* (nm) $\pm$ 0.005 $\pm$ 0.01
ZnO	31.71	(100)	0.2821	*Hexagonal*	$a = 0.324$
	34.37	(002)	0.2608		$c/a = 1.62$
Li-doped ZnO	31.71	(100)	0.2821	*Hexagonal*	$a = 0.325$
	34.38	(002)	0.2607		$c/a = 1.61$
Na-doped ZnO	31.71	(100)	0.2821	*Hexagonal*	$a = 0.325$
	34.35	(002)	0.2610		$c/a = 1.60$
K-doped ZnO	31.71	(100)	0.2820	*Hexagonal*	$a = 0.325$
	34.38	(002)	0.2608		$c/a = 1.61$

the undoped and doped ZnO NPs are summarized in Table 2. It can be seen that the physical parameters of the products are affected by the ionic size of dopant materials. However, ionic radii and reactivity of the dopant materials is a very important factor that should be considered. It is well known that the covalent power of the group-I elements decrease as you go down the column in the periodic table. Therefore, different results for these dopants could be due to from their different ionic radii and reactivity with oxygen.

3.2. Morphology studies

The TEM images and size distributions of the undoped and doped ZnO-NPs are shown in Fig. 3. It can be seen that the morphology of the nanostructures is nanoparticles. The minimum and maximum particle size is related to sample doping by K (Fig. 4(b)) and Li (Fig. 4(d)), respectively. The size distribution and histograms of the undoped and doped ZnO-NPs are shown beside the relative TEM images. The histograms indicate that the main particle sizes of the undoped and K-, Na- and Li-doped ZnO-NPs were about 105, 129, 132 and 150 nm, respectively. The obtained results from the TEM are in good agreement with the XRD results.

Elements of the periodic table with low Z ($Z < 11$) are not detectable by an energy-dispersive X-ray spectrometer (EDX) that usually is attached to a TEM. For this reason, field emission Auger electron spectrometer (FEAES) was used to study the products. Fig. 4(a–c) shows results of high-resolution N (E) Auger electron spectroscopy of lithium, sodium, and potassium, respectively. As illustrated in Fig. 4(a), a lithium peak at 36 eV is evident for the Li-doped ZnO-NPs. This corresponds to KLL Auger electron emission from the lithium. Fig. 4(b) shows a peak at 982 eV that indicates KLL Auger electron emission from the sodium. The FEAES spectrum of K-doped ZnO NPs is shown in Fig. 4(c). It includes a peak at 242 eV that corresponds to LMM Auger electron emission from potassium. The FEAES results show that the concentration of lithium, sodium and potassium is the same for all samples. Such peaks from the FEAES results and the XRD results provide strong evidence for successful Li-, Na, and K-doping in ZnO NPs.

Table 2
Geometrical and mechanical parameters of doped and undoped ZnO-NPs calcined at 650 °C.

Compound	*Size strain plotD* (nm)	$\varepsilon \times 10^{-4}$	$Y \times 10^{9}$	$\sigma \times 10^{6}$	$u \times 10^{3}$
ZnO	94	8.94	146	130.5	58.3
K-doped ZnO	107	8.94	146	130.5	58.3
Na-doped ZnO	115	6.32	146	92.3	29.2
Li-doped ZnO	125	2.82	146	41.2	5.8

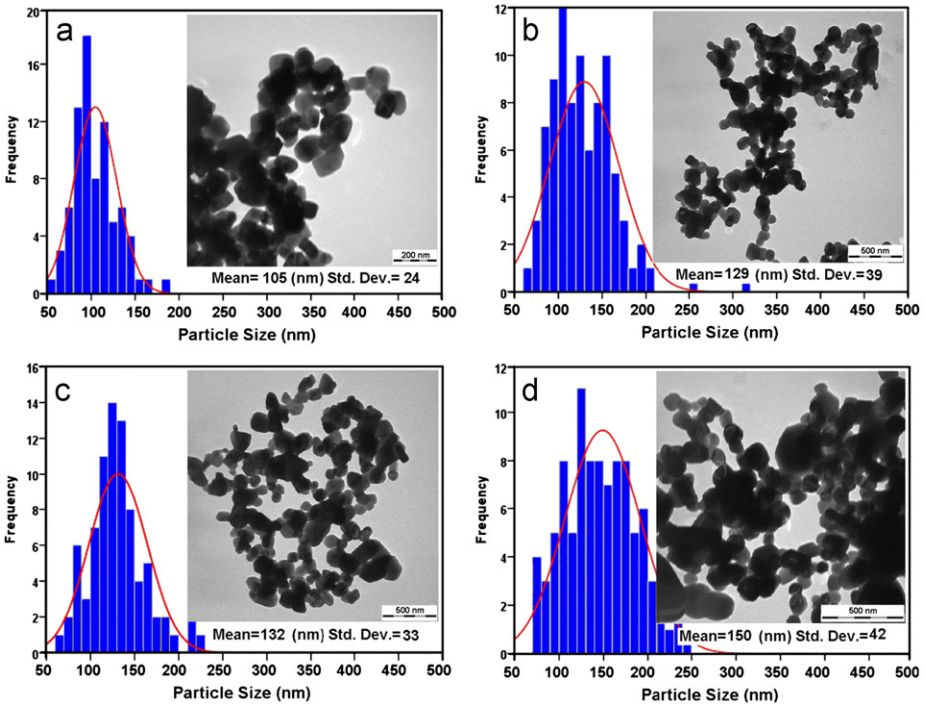

Fig. 3. TEM micrographs of doped and undoped ZnO-NPs calcined at 650 °C. (a) ZnO, (b) $Zn_{0.95}K_{0.1}O$, (c) $Zn_{0.95}Na_{0.1}O$, and (d) $Zn_{0.95}Li_{0.1}O$.

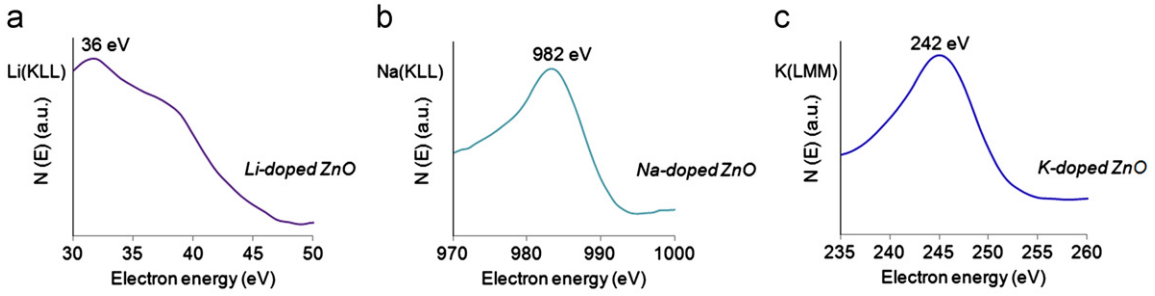

Fig. 4. High resolution N (E) Auger electron emission spectroscopy of the Li-doped, Na-doped, and K-doped ZnO nanoparticles: (a) Lithium spectrum corresponding to KLL Auger electron emission from lithium. (b) Sodium spectrum corresponding to KLL Auger electron emission from sodium. (c) Potassium spectrum corresponding to LMM Auger electron emission from potassium.

3.3. Optical properties

Raman spectroscopy is an effective technique for estimating the crystallinity of materials. According to the group theory, single crystalline ZnO belongs to the C_{6V}^4 space group having two formula units per primitive cell, and eight sets of optical phonon modes at the Γ point of the Brillouin zone, classified as $A_1+E_1+2E_2$ modes (Raman active), $2B_1$ modes (Raman silent) and A_1+E_1 modes (infrared active). The E_1 mode is a polar mode and is split into transverse optical (TO), and longitudinal optical (LO) branches. The Raman spectra for the undoped, Li-, Na-, and K-doped ZnO-NPs are shown in Fig. 5. As shown in Fig. 5, the Raman spectra of all the NPs show a sharp, strong, and dominant peak at 437 cm^{-1} corresponding to the E_2(high) mode of the Raman active mode, a characteristic peak for the wurtzite hexagonal phase of ZnO. A weak peak at 583 cm^{-1} corresponding to E_1(LO) is indicated for the undoped and doped ZnO-NPs. The E_1(LO) mode is associated with impurities and formation of defects such oxygen vacancies. Therefore, no visible E_1(LO) peak for the Li- and Na-doped ZnO NPs and the appearance of a weak E_1(LO) peak for the K-doped and undoped ZnO NPs indicate a higher crystalline quality and lower oxygen vacancy of the ZnO NPs. However, this result indicates that the Li- and Na-doped ZnO NPs have lower oxygen vacancies than K-doped and undoped ZnO NPs. In addition, Fig. 5 shows two peaks at 330 cm^{-1}, assigned to the $E_{2H}-E_{2L}$ (multi-phonon process) mode for the all samples. It is known that the $E_{2H}-E_{2L}$ can only be found when the ZnO is a single crystal.

Photoluminescence (PL) study is also a powerful method for investigating the effects of impurity doping on optical properties of semiconductor nanostructures with direct band gap, because doped nanostructures are expected to have different optical properties compare to undoped nanostructures. Fig. 6 shows the room temperature PL spectra of the undoped, Li-, Na- and K-doped ZnO NPs. All of the PL spectra of doped ZnO NPs show a strong peak in the ultraviolet (UV) region at 382 nm, and a weak green emission (deep-level emission) peaks in the visible region at ≈502–530 nm. On the other hand, the PL spectrum of the undoped ZnO NPs shows a stronger

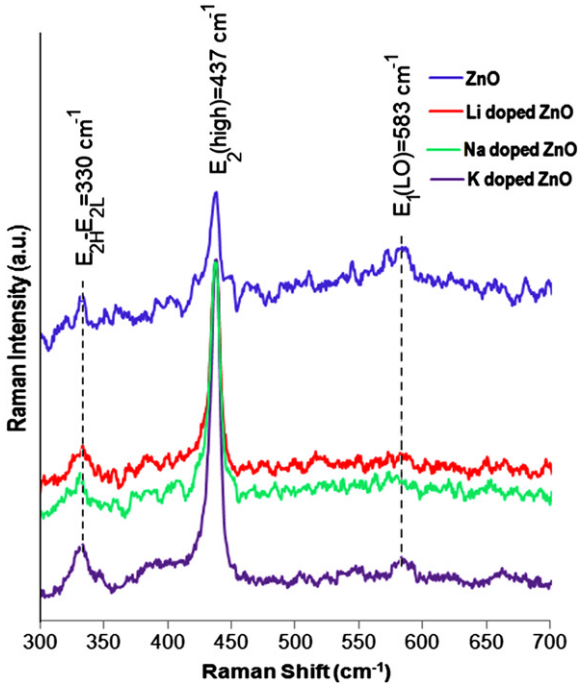

Fig. 5. Raman spectra of the undoped, Li-, Na-, and K-doped ZnO nanoparticles.

green emission peak than UV emission peak. This result indicates that the doped ZnO NPs have higher optical quality than undoped ZnO NPs. However, the PL results also reveal that Li-doped ZnO NPs have higher optical quality than the other ZnO NPs. These results are in good agreement with those obtained from the Raman results. Seemingly, the PL results indicate that group-I elements can reduce oxygen vacancies in ZnO lattice. However, more studies need to proof these results. The XRD results obtained from Table 2 show that the Li-doped ZnO NPs have significantly smaller stress than the other ZnO NPs. It is known that stress can decrease the crystalline and optical qualities of a sample [25]. However, the main reason to obtain these results could be ionic radii difference. Since Li (0.76 Å) has similar ionic radius with Zn (0.74 Å) in comparison to Na (1.02 Å) and K (1.38 Å) that have bigger ionic radii than Zn. The incorporation of guest element with big difference of ionic radius into the host lattice will

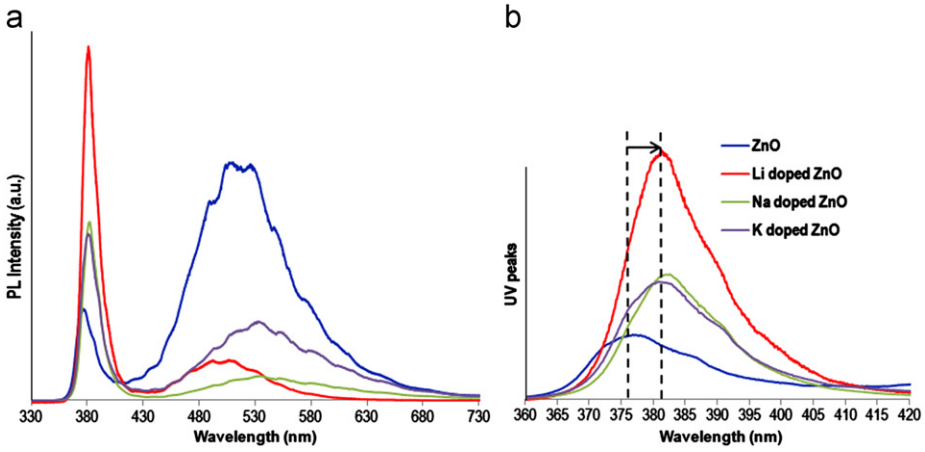

Fig. 6. (a) PL spectra of the undoped, Li-, Na-, and K-doped ZnO nanoparticles. (b) red-shift of the UV peaks for the doped ZnO nanoparticles compared to the undoped ZnO nanoparticles.

introduce lattice distortion. This effect influences the energy band structure of the ZnO NPs doped with sodium and potassium, and as a result, new defects such as oxygen vacancies can be introduced by the new band structure deformation. Compared with the undoped ZnO NPs, the PL spectra of the doped ZnO NPs show an obvious red-shift in the UV emission (Fig. 6(b)). This red-shift in the UV emission could be a result to obtain *p*-type ZnO NPs. A widening of the band-gap is usually observed for ZnO doped with donors; while *p*-type ZnO has shown band-gap reduction if doped with acceptors. In fact, the UV peak of the PL spectra of the ZnO nanostructures, which have been doped by donor materials, exhibited a blue-shift in comparison to that observed for the undoped ZnO nanostructures [26–28]. Our previous experiments about dopants materials as donors also confirm these results [6–9].

4. Conclusion

Undoped, Li-, Na-, and K-doped ZnO-NPs were synthesized by the sol–gel method in a gelatin media. The XRD results showed that all of the undoped and doped ZnO NPs exhibited the hexagonal with a wurtzite structure. The SSP method was used to calculate the crystallite size and strain of the undoped and doped lattices. The SSP results revealed that Li-doped ZnO NPs had smaller stress than the other ZnO NPs. The TEM and XRD results indicated that doping group-I elements help in the increase of the crystallite and particles sizes. The Raman results showed that Li-doped ZnO NPs had better crystalline quality than the other ZnO NPs. The PL results were in good agreement with those obtained from the Raman results. In addition, the PL results indicated that group-I elements as dopant materials could reduce oxygen vacancies in ZnO lattice. Furthermore, the UV peaks of the group-I doped ZnO NPs showed a red-shift in comparison to the undoped ZnO NPs. This red-shift could show the acceptor behavior of group-I elements in ZnO lattice.

Acknowledgment

This work was supported by the Islamic Azad University, Masjed-Soleiman Branch. R. Yousefi and F. Jamali-Sheini gratefully acknowledge the Islamic Azad University (I.A.U), Masjed-Soleiman and Ahwaz Branches, respectively, for their financial support in this research work.

References

[1] T.J. Minami, Transparent and conductive multicomponent oxide films prepared by magnetron sputtering, Journal of Vacuum Science and Technology A 17 (1999) 1765.
[2] A. Qurashi, M.F Hossain, M. Faiz, N. Tabet, M.W Alam, N.K Reddy, Fabrication of well-aligned and dumbbell-shaped hexagonal ZnO nanorod arrays and their dye sensitized solar cell applications, Journal of Alloys and Compounds 503 (2010) L40–L43.
[3] Y. Zong, Y. Cao, D. Jia, S. Bao, Y. Lu, Facile synthesis of Ag/ZnO nanorods using Ag/C cables as templates and their gas-sensing properties, Materials Letters 64 (2010) 243.
[4] F. Jamali-Sheini, K.R. Patil, Dilip S. Joag, Mahendra A. More, Synthesis of Cu–ZnO and C–ZnO nanoneedle arrays on zinc foil by low temperature oxidation route: effect of buffer layers on growth, optical and field emission properties, Applied Surface Science 257 (2011) 8366.
[5] M. Law, J. Goldberger, P. Yang, Semiconductor nanowires and nanotubes, Annual Review of Materials Research 34 (2004) 83.
[6] R. Yousefi, M.R. Muhamad, A.K. Zak, Investigation of indium oxide as a self-catalyst in ZnO/ZnInO heterostructure nanowires growth, Thin Solid Films 518 (2010) 5971.
[7] R. Yousefi, B. Kamaluddin, Effect of S- and Sn-doping to the optical properties of ZnO nanobelts, Applied Surface Science 255 (2009) 9376.
[8] R. Yousefi, M.R. Muhamad, Effects of gold catalysts and thermal evaporation method modifications on the growth process of $Zn_{1-x}Mg_xO$ nanowires, Journal of Solid State Chemistry 183 (2010) 1733.
[9] R. Yousefi, F.J. Sheini, M.R. Muhamad, M.A. More, Characterization and field emission properties of ZnMgO nanowires fabricated by thermal evaporation process, Solid State Sciences 12 (2010) 1088.
[10] K. Jayanthi, S. Chawla, K.N. Sood, M. Chhibara, S. Singh, Dopant induced morphology changes in ZnO nanocrystals, Applied Surface Science 255 (2009) 5869.

[11] J. Nayak, S. Kimura, S. Nozaki, Enhancement of the visible luminescence from the ZnO nanocrystals by Li and Al co-doping, Journal of Luminescence 129 (2009) 12.
[12] G.Y. Huang, C.Y. Wang, J.T. Wang, First-principles study of diffusion of Li, Na, K and Ag in ZnO, Journal of Physics: Condensed Matter 21 (2009) 345802.
[13] L. Li, C.X. Shan, B.H. Li, B. Yao, J.Y. Zhang, D.X. Zhao, Z.Z. Zhang, D.Z. Shen, X.W. Fan, Y.M. Lu, The compensation source in nitrogen doped ZnO, Journal of Physics D: Applied Physics 41 (2008) 245402.
[14] B. Yao, Y.P. Xie, C.X. Cong, H.J. Zhao, Y.R. Sui, T. Yang, Q. He, Mechanism of p-type conductivity for phosphorus-doped ZnO thin film, Journal of Physics D: Applied Physics 42 (2009) 015407.
[15] D. Yu, L. Hu, S. Qiao, H. Zhang, S.E.A. Len, L.K. Len, Q. Fu, X. Chen, K. Sun, Photoluminescence study of novel phosphorus-doped ZnO nanotetrapods synthesized by chemical vapour deposition, Journal of Physics D: Applied Physics 42 (2009) 055110.
[16] A. Janotti, C.G.V. Walle, Native point defects in ZnO, Physical Review B 76 (2007) 165202.
[17] E.C. Lee, K.J. Chang, Possible *p*-type doping with group-I elements in ZnO, Physical Review B 70 (2004) 115210.
[18] B. Xiao, Z. Ye, Y. Zhang, Y. Zeng, L. Zhu, B. Zhao, Fabrication of *p*-type Li-doped ZnO films by pulsed laser deposition, Applied Surface Science 253 (2006) 895.
[19] J.G. Lu, Y.Z. Zhang, Z.Z. Ye, L.P. Zhu, L. Wang, B.H. Zhao, Q.L. Liang, Low-resistivity, stable *p*-type ZnO thin films realized using a Li–N dual-acceptor doping method, Applied Physics Letter 88 (2006) 222114.
[20] A.K. Zak, M.E. Abrishami, W.H.A. Majid, R. Yousefi, S.M. Hosseini, Effects of annealing temperature on some structural and optical properties of ZnO nanoparticles prepared by a modified sol–gel combustion method, Ceramics International 37 (2011) 393.
[21] A.K. Zak, W.H.Abd. Majid, M.E. Abrishami, R. Yousefi, X-ray analysis of ZnO nanoparticles by Williamson-Hall and size-strain plot methods, Solid State Sciences 13 (2011) 251.
[22] B.D. Cullity, Elements of X-ray Diffraction, Addison-Wesley Publishing Company Inc., California, 1956.
[23] J.M. Zhang, Y. Zhang, K.-W. Xu, V. Ji, General compliance transformation relation and applications for anisotropic hexagonal metals, Solid State Communications 139 (2006) 87.
[24] J.F. Nye, Physical Properties of Crystals: Therir Representation by Tensors and Matrices, Oxford, New York, 1985.
[25] C. Kittel., Introduction to Solid State Physics, sixth ed., Wiley, New York, 1986.
[26] B. Nasr, S.D. Gupta, D. Wang, N. Mechau, R. Kruk, H. Hahn, Electrical resistivity of nanocrystalline Al-doped zinc oxide films as a function of Al content and the degree of its segregation at the grain boundaries, Journal of Applied Physics 108 (2010) 103721.
[27] M.A. Thomas, J.B. Cui, Electrochemical route to p-type doping of ZnO nanowires, The Journal of Physical Chemistry Letters 7 (2010) 1090.
[28] S. Shet, K.S. Ahn, Y. Yan, T. Deutsch, K.M. Chrustowski, J. Turner, M. Al-Jassim, N. Ravindra, Carrier concentration tuning of bandgap-reduced *p*-type ZnO films by codoping of Cu and Ga for improving photoelectrochemical response, Journal of Applied Physics 103 (2008) 073504.